JOURNAL OF MATERIALS SCIENCE 11 (1976) 1583–1592

The congruent melting composition of strontium barium niobate

K. MEGUMI, N. NAGATSUMA, Y. KASHIWADA, Y. FURUHATA
Central Research Laboratory, Hitachi, Ltd, Kokubunji, Tokyo 185, Japan

The congruent melting composition of strontium barium niobate has been investigated over the ternary composition region by DTA, X-ray fluorescence, Curie temperature and lattice parameter measurements. The composition of congruent melt was found to be close to $x = 0.61$, $y = 0.4993$ for the formula $(Sr_x Ba_{1-x} O)_{1-y} \cdot (Nb_2 O_5)_y$. Striation-free single crystals are grown from the melt with this composition. The conceivable reasons for the discrepancy between the results of this work and the previous data are briefly discussed.

1. Introduction

Strontium barium niobate ($Sr_x Ba_{1-x} Nb_2 O_6$) is a ferroelectric solid solution [1] with a tungsten bronze structure, which has lately become of major interest in the field of opto-electronics device application because $Sr_{0.75} Ba_{0.25} Nb_2 O_6$ has the largest electro-optic [2] and pyroelectric [3] coefficients of any well-behaved material. Acousto-optic [4] and non-linear [5] properties of this material also belong to the "A" class. Furthermore, much attention is now being paid to this material because it has great potential as a reversible optical storage medium controlled by an external electric field [6, 7].

The basic obstacle to the practical application of this excellent material is the difficulty in growing large single crystals with a good optical homogeneity. The main problems associated with the Czochralski growth of single crystals can be summarized as the instability of diameter and unavoidable optical inhomogeneity. The occurrence of "striation" which accounts for the inhomogeneity along the growth axis and "core" which causes the inhomogeneity along the direction normal to the growth axis, are included in the latter problem. Striation is the typical optical defect common to solid solution crystals and is quite difficult to suppress in the case of strontium barium niobate. One of the significant countermeasures to this problem is to grow crystals at the composition as close to a congruent melt as possible. Recently, a series of works to determine the accurate congruent melting composition has been successfully undertaken for the useful optic crystals, such as $LiNbO_3$ [8], $LiTaO_3$ [9] and BNN [10, 16], resulting in remarkable improvement with respect to crystal quality.

The $BaO–SrO–Nb_2O_5$ ternary phase diagram was initially proposed by Carruthers and Grasso [11]. Of all compounds existing in this system, strontium barium niobate (SBN) was investigated in detail to determine the existence region and the associated congruent melting composition. Present investigations are concerned with further refinements of this composition based on the results of Carruthers and Grasso. In the course of the precise determination of the congruent melting composition, a difference was found between the results of Carruthers and Grasso and ours. Therefore, three independent experiments to locate the congruent melting composition were carried out.

Fig. 1 shows the ternary phase relationship established by Carruthers and Grasso, which we took as a guide to the present work. The existence region of SBN is indicated by the hatched area. High temperature phase equilibria were also reported for the $BaNb_2O_6$(BN)–$SrNb_2O_6$(SN) system and 25% BaO isopleth. From these observations, Carruthers and Grasso concluded that the liquidus maximum of this solid solution should exist in the BN–SN psuedobinary, and the location of the congruent melting composition

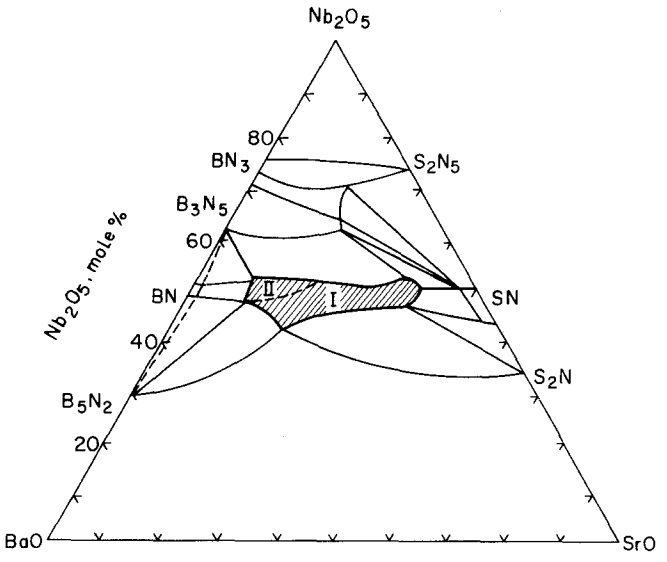

Figure 1 Ternary phase relationship in the room temperature isotherm of the system $BaO–SrO–Nb_2O_5$ proposed by Carruthers and Grasso [11]. Hatched area: solid solution area of SBN, phase II has the orthorhombic structure slightly distorted from tetragonal phase I.

($Sr_{0.46}Ba_{0.54}Nb_2O_6$) was determined by the results based on Curie temperature measurements for both ceramic and crystal speciments along this psuedobinary.

Ballman and Brown [12], and Brice *et al.* [13] independently reported composition shifts of crystals grown over the composition range from $Sr_{0.25}Ba_{0.75}Nb_2O_6$ to $Sr_{0.75}Ba_{0.25}Nb_2O_6$. However, their results were inconsistent with those of Carruthers and Grasso.

In this paper, the experimental techniques to locate the congruent melting composition of SBN in the ternary $BaO–SrO–Nb_2O_5$ region and the results are described. Assessment of the quality of Czochralski-grown crystals from the newly found congruent melt is presented in Section 3. Conceivable reasons for discrepancy between the results of this work and those of Carruthers and Grasso are discussed in Section 4.

2. Experimental techniques

The liquidus is extremely flat over a wide composition range along the BN–SN psuedobinary, as shown in the results of Carruthers and Grasso. Accordingly, measurements of melting temperature are not necessarily suitable for the accurate determination of a congruent melting composition. The alternative methods reported here are based on the comparison of melt composition with that of a crystal grown from the melt.

2.1. Sample preparation

All specimens were prepared from $SrCO_3$, $BaCO_3$ and Nb_2O_5 supplied by Johnson Matthey Chemical Co (specpure grade). Sufficiently mixed powders were pelletized and sintered in air at 1300 to 1400° C for 5 h. SBN single crystals were grown from melts in air using a Czochralski method with pulling rate of 10 mm h^{-1} and rotation speed of 60 rpm. The investigated composition region was $x = 0.40$ to 0.70 and $y = 0.48$ to 0.52 for the formula $(Sr_xBa_{1-x}O)_{1-y}.(Nb_2O_5)_y$, which is included in the solid solution area in Fig. 1.

Prior to Curie temperature and lattice parameter measurements, both ceramic and crystal specimens were re-heated at 1450° C for 6 h and then cooled to room temperature at a strictly uniform speed of 30° C h^{-1}.

2.2. Measurements

DTA measurements were performed on ceramic specimens using a Rigaku high temperature thermoanalyser with Pt capsules which were 8 mm in diameter, 16 mm in length and fabricated with 5 mm long Pt–Rh 13% thermocouple wells. α-Al_2O_3 served as a standard sample and the heating/cooling rate was 2.5° C min^{-1}.

Composition analysis of melts and crystals was chiefly carried out using a Rigaku fluorescent X-ray spectrometer with ceramic specimens as an analytical standard.

Dielectric constant measurements were made on 1 mm thick slices cut from both ceramic and crystal speciments using a capacitance bridge (Ando WBG–5) at 10 kHz with evaporated gold electrodes. Pyroelectric measurements were made on the same specimens by the static method using a vibrating reed electrometer (Takeda TR–84M).

The heating/cooling rate was kept strictly at 1° C min^{-1} in both experiments. All specimens were poled by the application of an electric field (about 20 kV cm^{-1}) at room temperature for 1 min before these electrical measurements.

Room temperature X-ray diffraction measurements were performed using a Rigaku spectrometer. Lattice parameters were calculated from 591 and 552–172 diffraction peaks through correction based on the Si internal standard.

Crystal homogeneity was assessed by examining the optically polished slices with a polarizing microscope and a Twyman–Green interferometer.

3. Experimental results

3.1. DTA measurements

Melting and crystallization temperatures were measured for the $Sr_xBa_{1-x}Nb_2O_6$ system. Although the liquidus temperatures agree for the most part with those reported by Carruthers and Grasso [11], the composition corresponding to maximum melting temperature seemed to be close to $x = 0.60$ rather than $x = 0.46$. In addition, the DTA curves taken at $x = 0.46$ always revealed doubly split patterns both in the heating and cooling cycles. This behaviour was observed in the whole solid solution range along the BN–SN psuedobinary.

Fig. 2 shows the difference between melting and crystallization temperatures compiled from DTA results. Such supercooling phenomena are usually observed in crystal growth experiments and their mechanisms are well understood, but the composition dependence of the degree of supercooling has never been reported to our knowledge.

A reasonable interpretation of this behaviour cannot be given at this stage. Nevertheless, it may be inferred that the degree of supercooling becomes maximal at the congruent melting composition from the fact that the degree of supercooling observed in the end members of this system is extremely large compared with that observed in other specimens in which heterogeneous nucleation occurs during the crystallization process.

These observations suggest that the congruent melting composition of SBN does not coincide with the proposed one and is slightly off the stoichiometric composition.

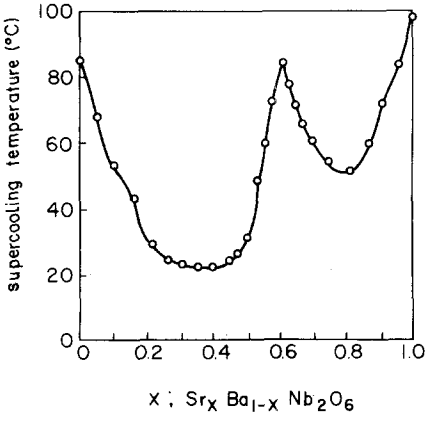

Figure 2 Supercooling temperatures as a function of melt composition.

3.2. Composition analysis by X-ray fluorescence

The composition of crystals grown up to about 10 wt % of the melts was examined using sufficiently reacted ceramic specimens as an analytical standard. A difficult matter encountered in this procedure was that X-ray intensity was affected by the inhomogeneity of grain size of specimens examined, especially in the case of Nb and Sr. The accuracy of this measurement was found to be greatly improved by making grain size uniform and using the Ba intensity and Nb/Sr intensity ratio as calibration curves, and it finally reached ± 0.1% for y and ± 0.2% for x.

In Fig. 3, the difference in composition between melts and crystals grown from them is shown. The origin of each arrow represents the original melt composition, while each arrow points toward the composition of the grown crystal. Each segment with an arrow head, therefore, corresponds to the liquidus–solidus tie line for a fixed composition. However, it should be noted that Fig. 3 does not represent the isotherm section. The composition shifts from melts to crystals change largely in magnitude, particularly with Nb_2O_5 concentration, and rotate from parallel to normal to the direction along the BN–SN psuedobinary. This implies that the solidus isotherms lack a point symmetry, taking an ellipse form extremely elongated along the BN–SN pseudobinary. The intersection of the shifts vectors in Fig. 3, e.g. $x = 0.40$, $y = 0.48$ and $x = 0.40$, $y = 0.49$, is considered to arise from the asymmetric shape of solidus isotherms since tenary liquidus–solidus tie lines move on three-dimensional surfaces with temperature.

The characteristic behaviour demonstrated in Fig. 3 leads us to the conjecture that the

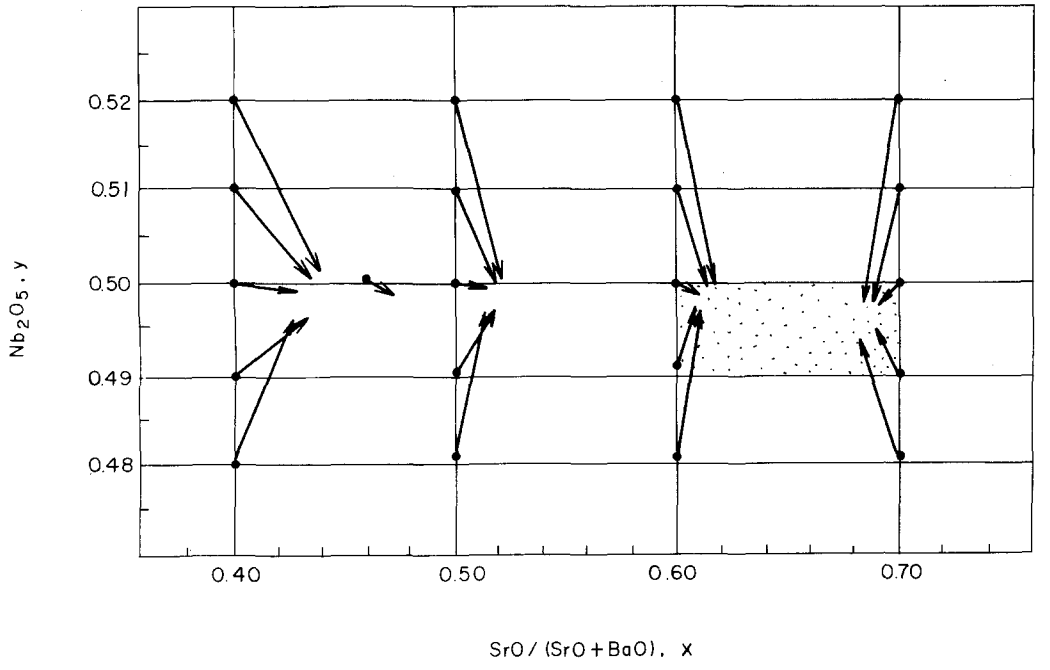

Figure 3 Composition shifts from melts to crystals. Dotted area: area containing congruent melting composition of SBN from present work.

congruent melting composition would lie within the region $x = 0.60$ to 0.70 and $y = 0.49$ to 0.50. This conclusion is supported, in part, by the photometric analysis shown in Fig. 4. The photometric method was barely valid for analysis of the Nb content, but not at all for the Sr or Ba content, on account of its conspicuous interference with other elements which compose SBN. An accuracy of only ± 0.5% was obtained for the Nb content. Nevertheless, the average value obtained by multiple experiments suggests that the Nb content relation between ceramics and crystals is reversed within the composition region under consideration.

The congruent melting composition was determined accurately by the following method. In this step, crystals were grown until the melts were almost consumed over the roughly estimated region. The residual melts left in the crucible were then completely gathered, sufficiently ground and their composition examined by the X-ray method mentioned above.

If a solid solution crystal growth is performed using an incongruent melt, the growing crystal changes its composition gradually, resulting in a corresponding change in the melt composition. As a result, the amount of composition shift of the melt from its earlier stage greatly exceeds that of the crystal from the melt at an earlier stage, when the solidified fraction of the melt, g is sufficiently large. This well-known behaviour in the growth of solid solution crystals could provide a powerful aid for accurate analysis.

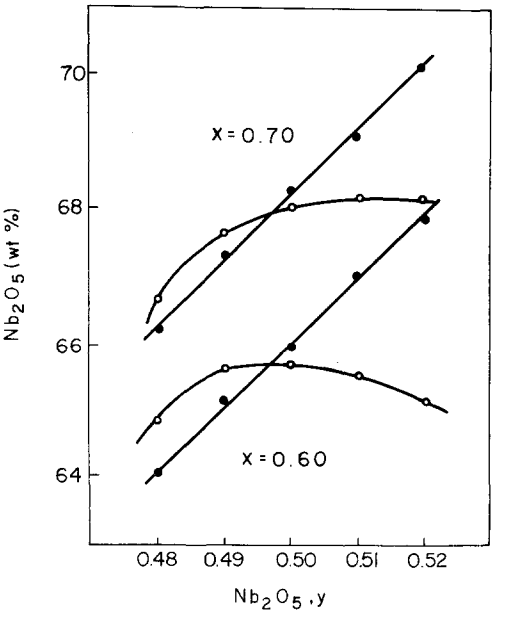

Figure 4 Analytical values by photometric method for Nb_2O_5. ○: crystal specimen results; ●: ceramic specimen results.

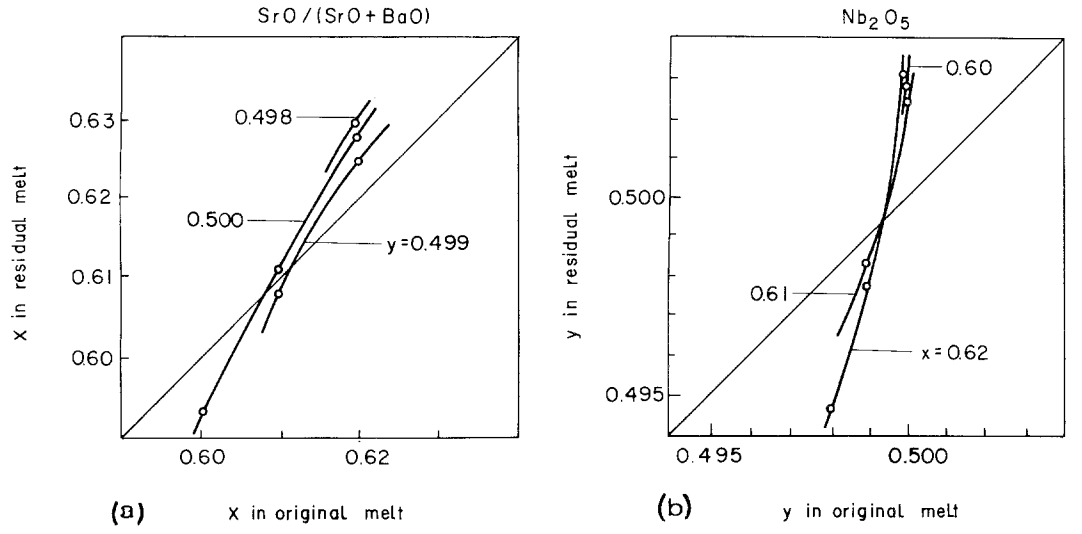

Figure 5 Compositional difference between original and residual melts. Solidified fraction of melts is about 0.80.

In Fig. 5, the results obtained on this conception are shown, where g is fixed at about 0.80. Fig. 5a and b represent the difference in composition between the original and residual melts in terms of the SrO/(SrO + BaO) ratio and Nb_2O_5 concentration, respectively. The datum curves for y are quite steep in comparison to those of x. This is because SBN possesses a little solubility on the Nb_2O_5-rich or deficient side of 50% Nb_2O_5, in contrast to a large existence region along the BN–SN psuedobinary, as shown in Fig. 3. This fact implies that the value of y can be determined more precisely than that of x. The congruent melting composition is denoted as a set of x and y values on the abscissas which can be obtained from the points where diagonally drawn lines intersect datum curves. The values thus obtained are $x = 0.610 \pm 0.002$ and $y = 0.4992 \pm 0.0002$.

3.3. Curie temperature measurements

The dielectric constants and pyroelectric coefficients of both ceramic and crystal specimens were measured. It was found that the peak temperatures of dielectric constant (T_c^d) and those of pyroelectric coefficient (T_c^p) did not agree with each other, as pointed out by Glass [3]. In addition, this Curie range shifted toward high temperature as the cooling rate was increased. Nevertheless, the relative change in peak temperatures with composition is useful if the cooling rate is kept constant in all experiments.

Fig. 6 shows the difference in dielectric peak temperature between ceramics and upper parts of crystals described in the preceding section. Crystal results are given in terms of melt composition. Pronounced variations of T_c^d were observed within the range of $y = 0.48$ to 0.50 for the ceramic specimens, whereas crystals had an almost unchanged T_c^d over a wide range. In Fig. 7, the results of measurements in the more detailed region of $x = 0.60$ to 0.65 and $y = 0.498$ to 0.501 are shown. The broken lines in these figures indicate the compositions where ceramics and crystals have the same T_c^d. Therefore, the congruent melting composition has to exist on these lines.

To examine the slight difference in peak temperature between the upper and lower parts of pulled crystals, pyroelectric measurements were effective since pyroelectric coefficient peaks were sharper than dielectric constant peaks. However, pyroelectric measurements were not valid for ceramic specimens since the results obtained lacked consistency. Fig. 8 shows the change of T_c^p with measured parts of crystals grown from melts with several compositions. The solid and broken lines represent the upper and lower part results, respectively. The points at which the solid lines intersect the broken lines correspond to the compositions where the upper and lower parts of crystals have the same T_c^p. The congruent melting composition is considered to exist on the line passing through these points.

Fig. 9 shows the results compiled from Figs. 7 and 8. The broken line shows the composition where ceramics and the upper parts of crystals

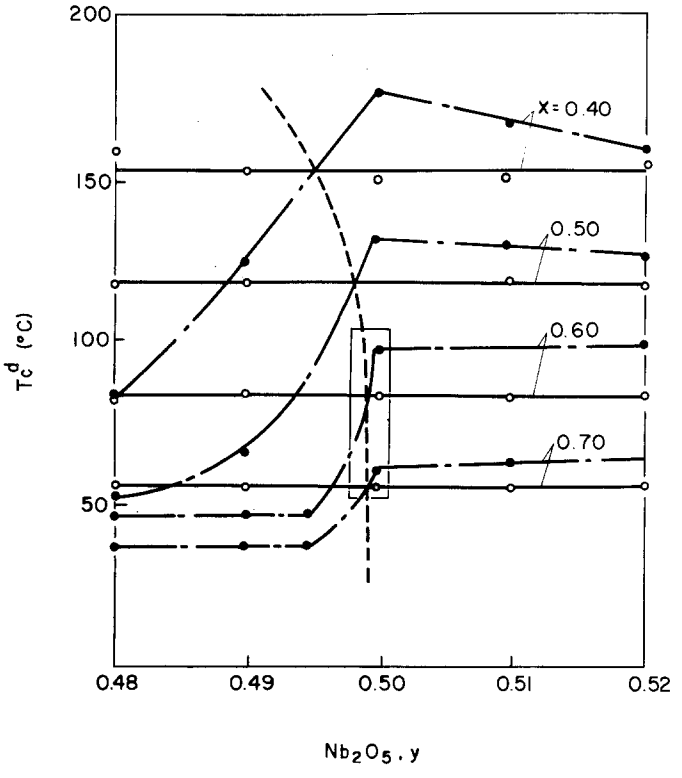

Figure 6 Curie temperatures (T_c^d) as a function of y. ○: crystal specimens; ●: ceramic specimens, ------; the composition where ceramic and crystal specimens have the same T_c^d.

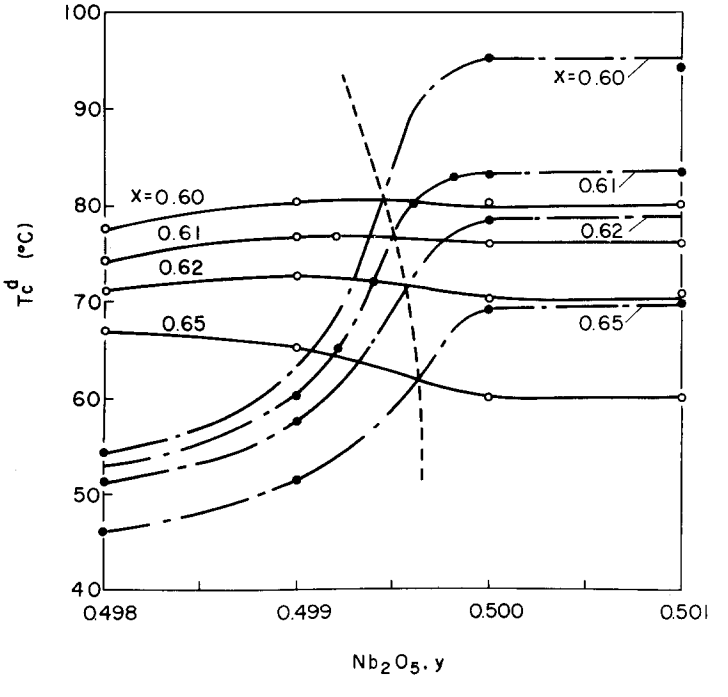

Figure 7 More detailed datum plots for the area framed by the solid line in Fig. 6.

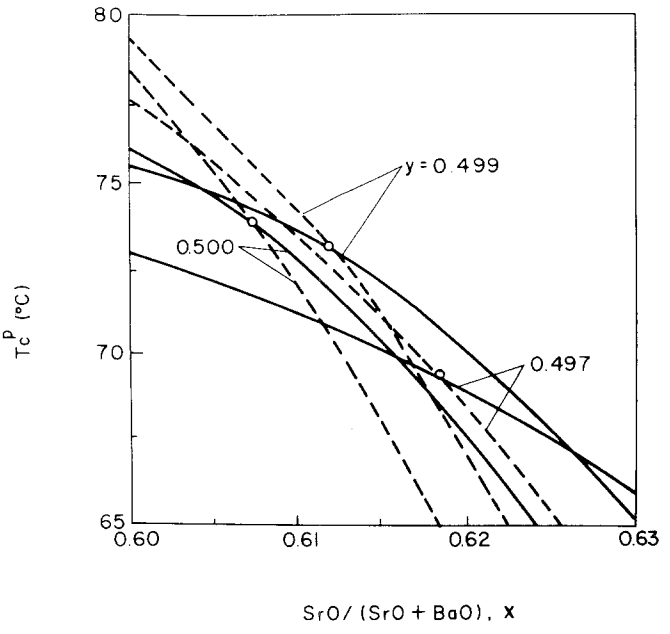

Figure 8 Curie temperatures (T_c^p) of upper and lower parts of crystals as a function of x. ———: upper parts; ------: lower parts; ○: the compositions where there is no difference in T_c^p between upper and lower parts of crystals.

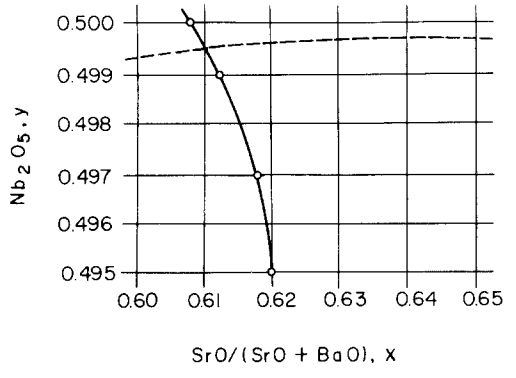

Figure 9 The compositions where ceramic and crystal specimens have the same T_c^d (------) and the upper and lower parts have the same T_c^p (———).

have the same T_c^d. The solid line indicates the composition where the upper and lower parts of crystals have the same T_c^p. Therefore, the congruent melting composition is given as the point where these two lines intersect. The value thus obtained is $x = 0.610 \pm 0.003, y = 0.4995 \pm 0.0003$.

3.4. Lattice parameter measurements

There have been a few reports on orthorhombic distortion from the tetragonal tungsten bronze structure [1, 11, 14]. In the experiments described here, such phenomena were also recognized in the specimens of which the composition was close to $x = 0.75, y = 0.50$. However, lattice parameters were calculated on the basis of the tetragonal structure since this treatment had insignificant effect on our purpose.

A similiar behaviour observed in Curie temperature measurements was found in this measurement. That is, the cooling rate much influenced lattice parameters. The larger the cooling rate was, the smaller the *a*-spacing and the larger the *c*-spacing became. Therefore, much attention was paid to the preparation of specimens treated under uniform cooling conditions.

In Fig. 10, the dependence of lattice parameters on ceramic specimen compositions is shown, where (a) is as a function of x and (b) a function of y. Both the *a*- and *c*-spacings decrease with the increase in the ratio of SrO/(SrO + BaO). On the other hand, the *a*-spacing decreases and *c*-spacing increases, when the content of Nb_2O_5 increases.

Fig. 11 represents the variation of lattice parameters in terms of ternary composition diagram, where the iso-*a* spacing lines are indicated by dot-dash lines and the iso-*c* spacing lines by solid lines. The composition dependences of lattice parameters definitely differ from each other, implying that the specimen compositions can be determined on the basis of lattice parameters alone. The lattice parameters had errors of ± 0.002 Å for the a-spacing and ± 0.001 Å for the *c*-spacing. The accuracy of the composition analysis based on Fig. 11 was limited by these errors to the following value: ± 0.012 for x, ± 0.010 for y.

Crystals were grown up to 75 wt % of the

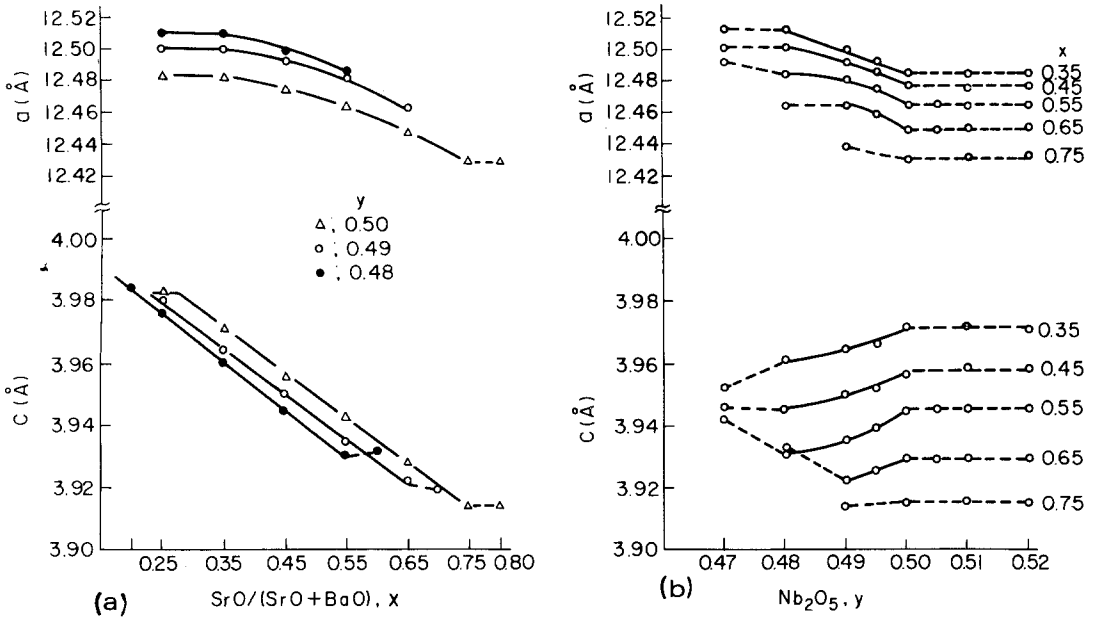

Figure 10 Lattice parameters as a function of composition (ceramic specimens).

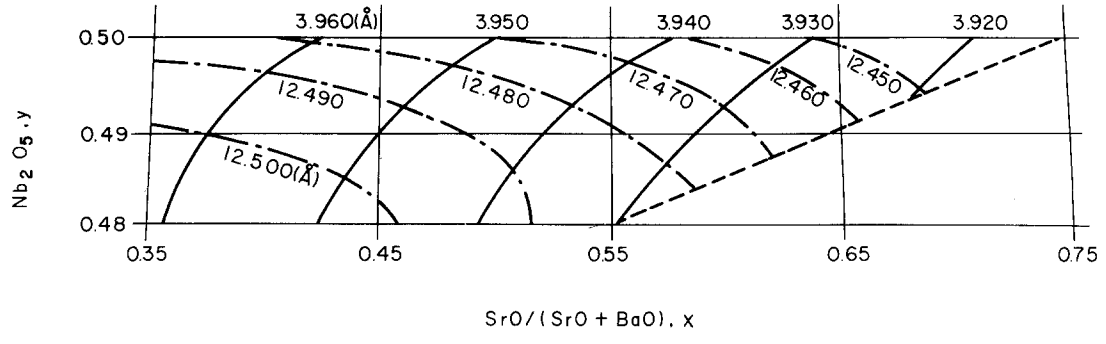

Figure 11 Iso-lattice parameter lines in SBN solid solution area. —.—.—: *a*-spacing, ———: *c*-spacing.

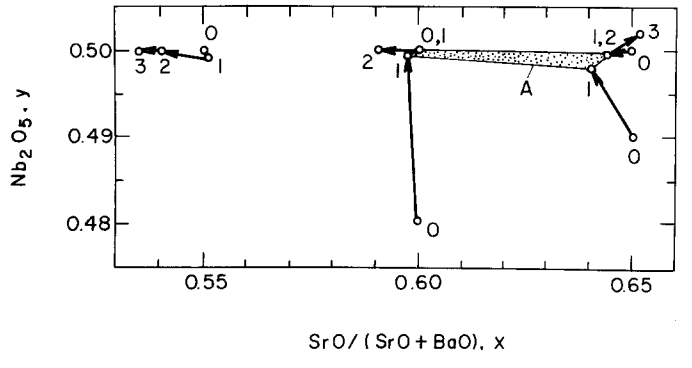

Figure 12 Composition shifts from original melts (0) to the upper parts of crystals (1), the lower parts of crystals (2) and residual melts (3).

melts, followed by composition analysis based on X-ray diffraction for the upper and lower parts of crystals and residual melts. In Fig. 12, the compositions of these specimens are shown, where the results obtained from the same melts are connected by each segment of a line with an arrow head. It is easily seen that "A" is the area in which the congruent melting composition should lie. In this area, further refinement was carried out using the crystals with solidified fraction $g = 0.95$. The

lower part of a crystal grown from a melt with a composition of $x = 0.60$, $y = 0.4995$ contained more Ba than the original melt, whereas a similiar specimen prepared from $x = 0.62$, $y = 0.4995$ contained less Ba than the original melt. However, the Nb contents in both specimens did not differ from those in the original melts. Analysis of another crystal prepared from $x = 0.61$, $y = 0.4995$ showed that the lower part of this crystal did not change at all in composition from its original melt. Thus, these observations show that the congruent melting composition is $x = 0.610 \pm 0.012, y = 0.4995 \pm 0.0010$.

3.5. Crystal growth observations

It is concluded from chemical and physical analyses that the congruent melting composition lies close to $x = 0.61$, $y = 0.4993$. Further confirmation of this conclusion was obtained from optical assessments and device performance.

Optically polished slices cut from crystals grown from the melt with this composition were examined with a polarizing microscope. Striation could not be found in the crystals, except those grown under the undesirable growth condition where the temperature fluctuation in the melt was larger then 10° C. The refractive index variations of such striation-free crystals were found to be smaller than 10^{-5} by means of a Twyman–Green interferometer. In addition, the extinction ratio of a light modulator made of such crystals was larger than 10^2.

4. Discussion

The congruent melting compositions based on various experiments are summarized in Table I. These data agree well with each other within the experimental error and are consistent with DTA and crystal growth observations.

Previous data (also included in Table I) proposed by Carruthers and Grasso [11] do not coincide with our results, but growth striations were observed in the crystals grown from the melt with the composition $Sr_{0.46}Ba_{0.54}Nb_2O_6$. Although this discrepancy is not understood at this stage, it may be associated with experimental methods, measurement accuracy and so on. Carruthers and Grasso's specimens were prepared from $Sr(NO_3)_2$, $Ba(NO_3)_2$ and Nb_2O_5, while ours were prepared from all carbonates and Nb_2O_5. It is possible that there is some difference in both specimens as to the completeness of the reaction.

Dielectric peak temperatures do not agree with pyroelectric peak temperatures in the case of SBN, which, as reported by Glass [3], is characterized by diffused phase transition. The pyroelectric peak is somewhat sharper than that of the dielectric constant. Therefore, the former is suitable for observation of slight differences in composition. It was also found that the dielectric properties were considerably influenced by the heat-treatment conditions, such as roasting temperature, period, and particularly cooling rate. Therefore, care was taken so that all specimens were treated under uniform conditions. Carruthers and Grasso reported heat-treatment conditions for ceramics but not for crystals. It is possible that there is some difference in their treatments between ceramics and crystals.

Concerning the shifts in T_c, Carruthers and Grasso reported that the rapid cooling gave rise to a decrease in T_c. However, our experiments showed opposite results, that is, T_c shifted towards higher temperature with the increase in the cooling rate. Although this discrepancy is not fully understood, our results seem to be supported by lattice parameter measurements (Section 3). The rapid cooling caused an increase in a-spacing together with a decrease in c-spacing, i.e. an increase in a/c axial ratio. This fact presumably supports T_c results, because Abrahams *et al.* [15] have shown that a linear relationship should exist

TABLE I The congruent melting compositions of SBN determined by various experiments.

x	y	Techniques	Investigators
0.610 ± 0.002	0.4992 ± 0.0002	X-ray fiuorescence	present work
0.610 ± 0.003	0.4995 ± 0.0003	Curie temp. (dielectric and pyroelectric)	present work
0.610 ± 0.012	0.4995 ± 0.0010	lattice parameters	present work
0.46 ± 0.04	0.5	DTA and Curie temp. (dielectric)q	Carruthers and Grasso [11]

between the spontaneous ferroelectric strain, X_s and the Curie temperature, T_c.

In all Curie temperature measurements we used Au electrodes alone since the dielectric properties of SBN depend strongly on electrode materials used, whereas Carruthers and Grasso used Pt and Au electrodes for ceramics and crystals, respectively. Their treatments may somewhat influence the determination of the relative changes in T_c from ceramics to crystals.

On the basis of DTA measurements for the BN–SN binary and 25% BaO isopleth specimens, Carruthers and Grasso concluded that melt compositions on the BN–SN binary join freeze along the binary join. Hence, they measured Curie temperatures for the BN–SN binary ceramic and crystal specimens to locate the congruent melting composition. However, their conclusions are inconsistent with our observations on composition shifts (Fig. 3) which indicate that the congruent melting composition is on the Nb_2O_5 deficient side of the BN–SN binary composition.

5. Conclusion

The congruent melting composition of strontium barium niobate was investigated over the ternary $BaO–SrO–Nb_2O_5$ composition region. The congruent melting compostion does not coincide with stoichiometric composition and its location is close to $x = 0.61, y = 0.4993$ for $(Sr_xBa_{1-x}O)_{1-y} \cdot (Nb_2O_5)_y$. Striation-free SBN single crystals could be grown from the melt with the congruent melting composition determined by this work.

Acknowledgements

The authors would like to thank Mr Y. Itoh for fruitful discussions and Mr H. Kozuka for growth of high quality crystals from the congruent melt.

References

1. M. H. FRANCOMBE, *Acta Cryst.* **13** (1960) 131.
2. P. L. LENZO, E. G. SPENCER and A. A. BALLMAN, *Appl. Phys. Letters* **11** (1967) 23.
3. A. M. GLASS, *J. Appl. Phys.* **40** (1969) 4699.
4. E. L. VENTIURINI, E. G. SPENCER and A. A. BALLMAN, *J. Appl. Phys.* **40** (1969) 1622.
5. S. C. ABRAHAMS, P. B. JAMIESON and J. L. BERNSTEIN, *J. Chem. Phys.* **54** (1971) 2355.
6. F. MICHERON, C. MAYEUX and J. C. TROTIER, *Appl. Optics* **13** (1974) 913.
7. J. B. THAXTER and M. KESTIGIAN, *ibid* **13** (1974) 913.
8. J. R. CARRUTHERS, G. E. PETERSON and M. GRASSO, *J. Appl. Phys.* **42** (1971) 1846.
9. S. MIYAZAWA and H. IWASAKI, *J. Crystal Growth* **10** (1971) 276
10. K. G. BARRACLOUGH, I. R. HARRIS, B. COCKAYNE, J. G. PLANT and A. W. VERE, *J. Mater. Sci.* **5** (1970) 189.
11. J. R. CARRUTHERS and M. GRASSO, *J. Electrochem. Soc.* **117** (1970) 1426.
12. A. A. BALLMAN and H. BROWN, *J. Crystal Growth* **1** (1967) 311.
13. J. C. BRICE, O. F. HILL, P. A. C. WHIFFIN and J. A. WILKINSON, *ibid* **10** (1971) 133.
14. I. G. ISMAILZADE, *Kristallografia* **5** (1960) 268.
15. S. C. ABRAHAMS, S. K. KURTZ and P. B. JAMIESON, *Phys. Rev.* **172** (1968) 551.
16. J. R. CARRUTHERS, S. L. BLANK, M. GRASSO and W. A. BIOLSI, *J. Crystal Growth* **23** (1974) 195.

Received 5 March and accepted 22 March 1976.